UNIVERSITÀ DEGLI STUDI FIRENZE

FLORE
Repository istituzionale dell'Università degli Studi di Firenze

Do alternate bars affect sediment transport and flow resistance in gravel-bed rivers?

Questa è la Versione finale referata (Post print/Accepted manuscript) della seguente pubblicazione:

Original Citation:

Do alternate bars affect sediment transport and flow resistance in gravel-bed rivers? / S.Francalanci; L.Solari; M.Toffolon; G.Parker. - In: EARTH SURFACE PROCESSES AND LANDFORMS. - ISSN 0197-9337. - STAMPA. - 37:(2012), pp. 866-875. [10.1002/esp.3217]

Availability:

This version is available at: 2158/594709 since: 2016-01-20T12:42:49Z

Published version:

DOI: 10.1002/esp.3217

Terms of use:

Open Access

La pubblicazione è resa disponibile sotto le norme e i termini della licenza di deposito, secondo quanto stabilito dalla Policy per l'accesso aperto dell'Università degli Studi di Firenze (https://www.sba.unifi.it/upload/policy-oa-2016-1.pdf)

Publisher copyright claim:

(Article begins on next page)

18 May 2024

EARTH SURFACE PROCESSES AND LANDFORMS
Earth Surf. Process. Landforms **37**, 866–875 (2012)
Copyright © 2012 John Wiley & Sons, Ltd.
Published online 12 March 2012 in Wiley Online Library
(wileyonlinelibrary.com) DOI: 10.1002/esp.3217

Do alternate bars affect sediment transport and flow resistance in gravel-bed rivers?

Simona Francalanci,[1]* Luca Solari,[2] Marco Toffolon[3] and Gary Parker[4]
[1] CERAFRI – Center of Research and Advanced Education for Hydrogeological Risk Prevention, Retignano di Stazzema, (Lu) Italy
[2] Department of Civil and Environmental Engineering, University of Florence, Firenze, Italy
[3] Department of Civil and Environmental Engineering, University of Trento, Trento, Italy
[4] Department of Civil and Environmental Engineering and Department of Geology, University of Illinois, Urbana, IL USA

Received 30 January 2011; Revised 11 November 2011; Accepted 16 January 2012

*Correspondence to: Simona Francalanci, Center of Research and Advanced Education for Hydrogeological Risk Prevention, via XI Febbraio, 55040 Retignano di Stazzema (Lu), Italy. E-mail: simona.francalanci@dicea.unifi.it

ESPL
Earth Surface Processes and Landforms

ABSTRACT: In natural gravel-bed streams, the complex topography of the bed can cause variation of flow resistance and sediment transport. Previous studies have shown that in addition to grain resistance (skin friction), flow resistance is also caused by bank roughness, channel bars, bed undulations and channel curvature. Sediment transport is similarly influenced by the complex topography, and the transport rate can vary spatially. A three-dimensional (3D) numerical model was used to generate a detailed description of the flow and bedload transport fields in gravel-bed rivers. Here we quantify the reach-averaged hydraulic resistance and sediment transport regime that prevails when self-formed alternate river bars are present, and compare with the regime that would prevail were no bars are present. We do this by comparing the results of (i) a 3D morphodynamic model in which bars form as a consequence of flow-bed interaction and (ii) an 'equivalent' one-dimensional (1D) case, which refers to flat bed conditions, but otherwise corresponding to identical average velocity and bed slope. The 3D numerical model is applied to generate different bed topographies of alternate bars at regime morphological equilibrium, then extended to non-equilibrium conditions for decreasing shear stress within a sensitivity analysis context. The contribution of grain resistance is estimated with the local values of the bed shear stress, while bar resistance results from the overall deviation of the flow field from that occurring in the flat bed configuration. The local sediment transport in both the longitudinal and transverse directions is computed with the local Shields stress and local bed inclination. The calculations result in a method for correcting 1D models to account for the total sediment transport and resistance in a cross-section due to 3D effects of alternate bars. We term the resulting relations 'morphologically averaged' sediment transport and resistance equations. Copyright © 2012 John Wiley & Sons, Ltd.

KEYWORDS: bedload transport; gravel-bed rivers; alternate bars; morphodynamics

Introduction

Gravel-bed rivers are often characterized by complex bed topography, including single- and multiple-row alternate bars, bed undulations associated with channel curvature, riffle and pool sequences, braiding, etc. All these features affect the local structure of the flow field, and thus hydraulic resistance (see for instance Kaufmann *et al.*, 2008). According to the classical approach of Einstein (1950), when bedforms are not present the drag on the bed that drives bedload transport is provided solely by skin friction. It has also been shown that, when bedforms such as dunes are present, the resistance exerted by the bed on the flow can be significantly larger than that due to skin friction only. The excess, i.e. form drag, is generally treated as not contributing to bedload transport.

In a gravel-bed river, the most common bed morphology consists of alternating diagonal bars. Dunes can be present in such streams (Dinehart, 1989), but seem to be relatively rare. Parker and Peterson (1980) suggest that in gravel-bed streams bars are formed almost exclusively at flood stages, when the bar pattern itself appears to contribute only modestly to resistance. Millar (1999), Parker (2008) and Parker *et al.* (2007), however, argue for the presence of some form of drag during formative flows.

In the case of macroscale bedforms such as bars, Parker and Peterson (1980) used the basic ideas developed by Einstein and Barbarossa (1952) for sand-bed streams and separated bed resistance into grain resistance (associated with particle size) and bar resistance, that is the form drag due to bed undulations. This approach has been adopted by several authors such as Bathurst (1981) and Prestegaard (1983).

Similarly to flow resistance, it is expected that sediment transport capacity is affected by the complex morphology as well. In particular, sediment transport predictors are invariably non-linear in their primary driving parameter, e.g. Shields number. That is, a doubling of Shields number produces more than a doubling of the load. This effect is particularly strong at low transport rates. Following the approach provided by Paola and Seal (1995), in a natural channel with bars, bends and other elements of channel complexity, local skin friction can

be expected to vary spatially according to some probability distribution. The same holds true for local mean grain size, and thus for the Shields number based on skin friction itself. The more complex the channel is, the higher will be the standard deviations of these fluctuations. In a non-linear transport relation, zones of high Shields number will magnify the transport rate far more than zones of low Shields number depress it. The result is to elevate the overall transport rate, compared to a uniform channel with spatially constant mean grain shear stress. In addition, if the transport relation is grain size-specific and renders finer surface grains more mobile than coarser surface grains, the effect of non-linearity can also act to bias the load towards the fine grains, especially in the case of relatively low boundary shear stress. The experimental observations of Lanzoni (2000b) and Madej *et al.* (2009) shed light on this phenomenon.

The main aim of this work is to quantify whether and how much the presence of a complex three-dimensional (3D) morphology due to alternate bars in a straight channel may generate an additional contribution to total drag resistance and sediment transport, as compared to the equivalent one-dimensional (1D) case of a flat and straight bed, having the same channel slope and average flow velocity. To this aim, a 3D hydro-morphodynamic model is applied to reproduce alternate bar patterns. The resulting sediment transport and flow resistance patterns are then averaged over the bar wavelength and compared to the equivalent 1D case. The overall effect of the alternate bars is embodied in 'morphological factors' correcting the classical equations for flow resistance and sediment transport originally developed for 1D flat geometries. These 'morphological factors' can be easily incorporated in 1D models for hydro-morphodynamic computations. Note that Blanckaert and de Vriend (2003) and Blanckaert (2009) proposed an analogous correction factor to the flow resistance that allows accounting for curvature-induced 3D hydrodynamics effects in 1D models.

The rest of the paper is organized as follows: in the next section we state the problem of deriving 'morphological factors' for flow resistance and bedload transport in gravel-bed rivers; in the third section we highlight the main results of this work, and discuss them in more detail in the fourth section; and finally we draw our conclusions. In Appendix A we solve the problem of flow resistance and sediment transport in two schematic cases which are helpful in interpreting our results.

Formulation of the Problem

We consider a straight river reach with complex topography and mean streamwise slope S. Neglecting the direct influence of the bank regions on the central flow, as commonly done in simplified analyses, we abstract the problem in terms of the conceptual sketch of Figure 1, where h is local water level and η is local bed level (both defined with respect to a reference plane inclined with the mean slope S), $H = h - \eta$ is local depth, U is depth-averaged velocity, τ is bed shear stress, and q is streamwise sediment transport per unit width. All variables are local, and thus functions of both the transverse coordinate y and longitudinal coordinate x. We assume macroscopic steady state conditions (i.e. averaged over periodic topography) with a constant discharge Q. Given the local channel width B and the cross-section area A for any position x, we introduce reach-averaged variables as follows:

$$\bar{A} = \frac{1}{L}\int_L \int_{B(x)} H(x,y)dydx\,, \quad \bar{B} = \frac{1}{L}\int_L B(x)dx \tag{1}$$

$$\bar{H} = \frac{\bar{A}}{\bar{B}} = \frac{1}{\bar{B}L}\int_L \int_{B(x)} H(x,y)dydx, \tag{2}$$

$$\bar{\tau} = \frac{1}{\bar{B}L}\int_L \int_{B(x)} \tau(x,y)dydx, \tag{3}$$

$$\bar{U} = \frac{Q}{\bar{A}} = \frac{1}{\bar{B}\bar{H}L}\int_L \int_{B(x)} U(x,y)H(x,y)dydx, \tag{4}$$

$$\bar{q} = \frac{1}{\bar{B}L}\int_L \int_{B(x)} q(x,y)dydx. \tag{5}$$

with L being the characteristic wavelength of bed deformation (see Figure 1b). The aspect ratio $\beta = (B/2)/\bar{H}$ is defined using the half width, so as to be comparable with previous studies (e.g. Colombini *et al.*, 1987).

Considering an equilibrium steady flow over such a bed, these definitions allow for the introduction of an effective total drag coefficient in the form

$$C_t = \frac{\bar{\tau}}{\rho\bar{U}^2}, \tag{6}$$

which we hypothesize can be expressed in terms of the averaged variables defined earlier.

Therefore, we compare the flow over a bed with complex topography to an equivalent flat bed in an ideal condition (i.e. a prismatic reach without transverse variations and with constant longitudinal slope), but characterized by the same values of microscopic roughness (skin friction), bed slope S and mean velocity $\bar{U}$. We indicate this configuration with a subscript s, which stands for 'skin', since the resistance must be completely associated with skin friction in the absence of local variation. In this case, the mean bed shear stress for the equivalent flat bed condition is expressed as

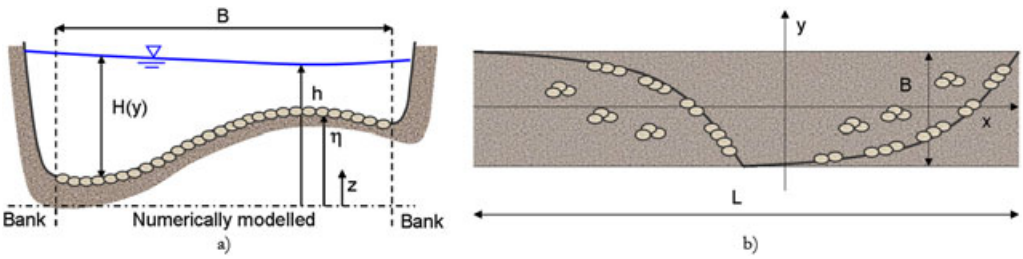

Figure 1. (a) Sketch of the cross-section and notations; (b) plan view. This figure is available in colour online at wileyonlinelibrary.com/journal/espl

Copyright © 2012 John Wiley & Sons, Ltd.

$$\tau_s = \rho g H_s S = \rho C_s \bar{U}^2, \tag{7}$$

where H_s is the equivalent flow depth (Figure 2), and C_s is the skin friction coefficient, which can be estimated using a suitable empirical relationship, such as (Parker, 1991):

$$C_s^{-1/2} = 8.1\left(\frac{H_s}{2 \cdot D_{90}}\right)^{1/6}, \tag{8}$$

where D_{90} is the grain size such that 90% of the mass fraction in the sample is finer.

At the same flow velocity $\bar{U}$ and bed slope S, the skin friction coefficient C_s and the flow depth H_s are, in general, different from the values corresponding to the case where bedforms are present. For instance, when dunes form, it is well known that the drag coefficient increases (Einstein and Barbarossa, 1952; Engelund and Hansen, 1967), determining larger flow depth. In the case of large-scale bedforms this is not so obvious. (See the case of a prismatic channel with variable cross-section discussed in Appendix A.) Here we build a rational framework for the analysis of this case. (Note that in addition to our approach, the equivalence with the flat bed could also be considered by matching the mean depth $\bar{H}$, or the flow discharge Q, in addition to S.)

Hence, given the depth $\bar{H}$ and velocity $\bar{U}$ averaged over the reach, the bed shear stress can be expressed using a normal flow relation:

$$\bar{\tau} = \bar{\chi}\rho g \bar{H} S = \rho C_t \bar{U}^2, \tag{9}$$

where $\bar{\chi}$ is a factor accounting for the cross-sectional shape associated with bars (see Appendix A), such that $\bar{\chi}\bar{H}$ is the hydraulic ratio of the cross-section.

Following Einstein (1950), we can compare Equation 9 with Equation 6, calculated for the same mean velocity $\bar{U}$ and the same slope S, and separate the two contributions characterizing the total bed resistance by introducing $H_f = \bar{\chi}\bar{H} - H_s$, which represents the variation of the depth associated with bar resistance, and τ_f, which is the mean bed shear stress due to bar resistance (with the subscript f standing for 'form' drag):

$$\tau_f = \rho g H_f S = \rho C_f \bar{U}^2. \tag{10}$$

Then, adding Equations 7 and 10 and comparing to Equation 9, it follows that

$$\bar{\tau} = \rho(C_s + C_f)\bar{U}^2 = \rho g H_s S + \rho C_f \bar{U}^2 = \rho g \bar{\chi}\bar{H} S, \tag{11}$$

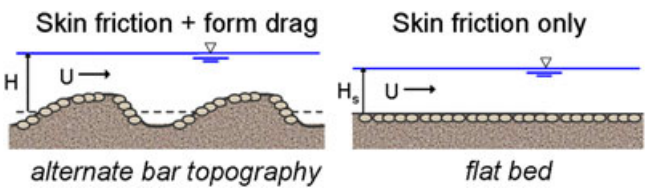

Figure 2. Comparison between the case of complex morphology and a corresponding flat bed. This figure is available in colour online at wileyonlinelibrary.com/journal/espl

$$C_f = \frac{g(\bar{\chi}\bar{H} - H_s)S}{\bar{U}^2}. \tag{12}$$

The latter equation provides an operative way to evaluate the additional contribution of resistance due to the complex morphology of the bed.

In general, the total drag coefficient estimated from Equation 6 can be expressed as a correction k_c of the coefficient calculated with the average quantities according to empirical relationships such as Equation 8, i.e.

$$C_t = k_c \cdot C_s(\bar{H}, D_{90}). \tag{13}$$

Analogous considerations can be made for the bedload transport relation. Let us assume a generic form

$$q = b \cdot \left(\tau^* - \tau^*_{cr}\right)^n \tag{14}$$

where b is a constant, $\tau^* = \tau/(\rho g s_g D)$ denotes the dimensionless Shields number, τ^*_{cr} the critical Shields number, and the exponent n is in general expected to be greater than unity. In most practical cases, where only 1D information is used, the value of the bedload is implicitly taken to be 'averaged over a bar pattern', and is thus extracted here from the more general analysis using spatial averages (i.e. bed shear stress $\bar{\tau}^*$, depth $\bar{H}$, and sediment diameter $\bar{D}$). It is apparent that, given the non-linear structure of typical bedload formulas, this estimate does not correspond to the spatial average $\bar{q}$ of the local values of the bedload, which depends on the local hydrodynamics and morphology (bed grain size distribution and local bed inclinations). In analogy with Equation 13, then, we introduce a correction coefficient k_q in the relationship for bedload transport, as follows:

$$\bar{q} = k_q \cdot q(\bar{\tau}*, \bar{H}, \bar{D}, etc.). \tag{15}$$

In the calculations presented here, we assume that $n = 3/2$, i.e. the value for the Meyer-Peter and Müller (1948) relation; see also Wong and Parker (2006). In the following sections, we evaluate the correction coefficients k_c and k_q by comparing the spatial averages over a bar wavelength of the local values, determined by means of a 3D model, of drag coefficient and bedload with the estimates obtained using the spatially averaged values of the hydrodynamic variables. In particular, results will show how the correction factors change as functions of changing discharge, water level or flow velocity. Since the relevant spatial averages of 3D information over the bar pattern represent the sediment transport rate and bed resistance at macroscopic (bar-averaged) scale, we term the resulting correction coefficients k_c and k_q as 'morphological factors'.

Results

We used the hydro-morphodynamic model developed by Vignoli (2005) to reproduce alternate-bar pattern in a straight channel. This model solves the 3D Reynolds-averaged equations under the commonly used assumption of shallow water, together with a mass balance Exner equation for the sediment. The effect of the banks is neglected. The model has been shown to adequately represent the hydrodynamics of fluvial systems and the role of sediment transport in the development of bed topography (Vignoli and Tubino, 2002; Toffolon and Vignoli, 2007), and has been used previously by the authors to investigate the effect of high local slopes on sediment transport and bed forms dynamics (Francalanci *et al.*,

Copyright © 2012 John Wiley & Sons, Ltd.

2009). In the numerical model, the bedload transport is evaluated with the non-linear equations of Francalanci and Solari (2008) devised for evaluating sediment transport in gravel-bed rivers in the case of arbitrarily local bed inclinations in both the longitudinal (α) and transverse (φ) direction. The local flow resistance is evaluated through Equation 8, which is a Manning–Strickler type relation proposed by Parker (1991) and tested by Wong and Parker (2006) on data pertaining to mobile-bed conditions in laboratory flumes, for which bedforms were absent (Meyer-Peter and Müller, 1948).

The parameters to be set in the numerical simulations are the particle Reynolds number R_p, the aspect ratio β, a wave number λ_D, corresponding to the length L_D of the domain, the Shields number τ^*, and the channel slope S:

$$R_p = \frac{\sqrt{(s_g - 1)gD^3}}{\nu} \tag{16}$$

$$\beta = \frac{B/2}{\bar{H}} \tag{17}$$

$$\lambda_D = \frac{2\pi}{L_D}\frac{B}{2} \tag{18}$$

where s_g is relative density of sediment, D is a characteristic sediment diameter and ν is kinematic viscosity of fresh water.

Although the bars in the model are self-formed, cyclic boundary conditions require that an integral number of bars fit within the computational domain; thus if L is bar wavelength, the bar wavenumber is given as

$$\lambda = \frac{2\pi}{L}\frac{B}{2} = \lambda_D n_b \tag{19}$$

where n_b is the number of bars that develop in the periodic domain.

The 3D model is used here to perform a systematic set of numerical runs to generate alternate bars at bankfull conditions that are in macroscopic equilibrium with the imposed flow discharge, channel geometry and bed grain size. The parameters employed in the various simulations are reported in Table I. The aspect ratio β, which ranges from 18 to 30, has been chosen to be sufficiently high to allow the development of alternate bars. The bed sediment size is maintained constant in all the simulations at 2 cm; and the relative submergence (defined as $\bar{H}/D$) is in the range 16–82. The bankfull Shields parameter is in the range 0·05–0·2 for channel slopes between 0·1% and 2%. These latter values are compared with the data set proposed by Parker *et al.* (2007) (see Figure 3); it appears that the adopted values of the parameters are within the typical range found in gravel-bed rivers.

Figure 4 shows, as an example, the equilibrium alternate-bar topography obtained with the numerical model. In Figure 4 η

Table I. Dimensionless parameters used in numerical simulations.

R_p	λ_D	β	(τ^*, S)
11000	0·2	18	(0·05, 0·001); (0·1, 0·005); (0·15, 0·01); (0·2, 0·02)
11000	0·2	24	(0·05, 0·001); (0·1, 0·005); (0·15, 0·01); (0·2, 0·02)
11000	0·2	30	(0·05, 0·001); (0·1, 0·005); (0·15, 0·01); (0·2, 0·02)
11000	0·1	18	(0·05, 0·001); (0·1, 0·005); (0·15, 0·01); (0·2, 0·02)
11000	0·4	18	(0·05, 0·001); (0·1, 0·005); (0·15, 0·01); (0·2, 0·02)

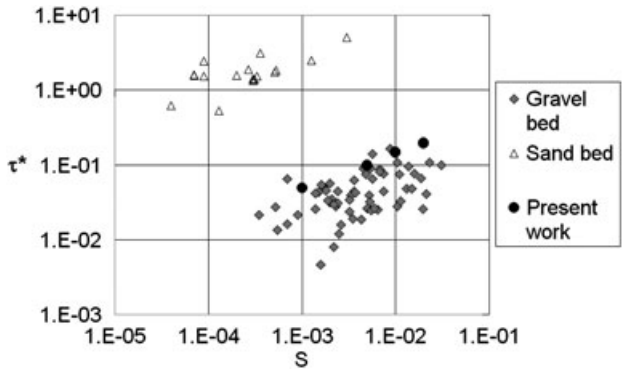

Figure 3. Dimensionless parameters characterizing channel bankfull geometry of gravel-bed rivers (Parker *et al.*, 2007): Shields number versus channel slope. The parameters used in the numerical simulations of the present work are added for comparison.

and x have been made dimensionless with the reference water depth, and y has been made dimensionless with channel width; the notation '*' denotes a dimensionless variable.

The horizontal velocity flow field is shown, superimposed over the bottom topography, both close to the bed ($z^* = 0{\cdot}005$) and at the water surface ($z^* = 1$). It is seen that the flow velocity direction is influenced by the steep slope of the diagonal bar front. This forces the flow to deviate from one side to the other (similarly to the case of a riffle-and-pool sequence). The deviation of velocity vectors is higher close to the bed. The cross-sectionally averaged values of total resistance C_t and sediment transport q are shown in Figure 5 for the same equilibrium configuration. It is seen that the local resistance is appreciably varying along the cross-section and the bar length, but that the cross-sectional average flattens the oscillations. In addition, the local bedload transport rate ranges from very low values close to incipient motion to much higher ones, but the cross-sectionally averaged value is only slightly varying around the mean.

In order to investigate the flow resistance and sediment transport when the flow discharge is smaller than the bankfull value, the alternate-bar patterns numerically reproduced using the input parameters in Table I, are 'frozen', and the flow

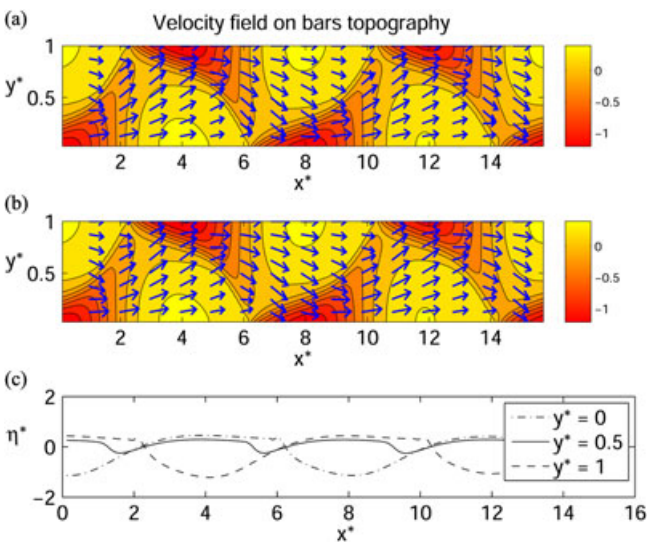

Figure 4. Example of an alternate bar topography at regime morphological equilibrium: color bar shows bed elevation while the arrows indicate the horizontal velocity field (a) close to the bed and (b) at the water surface; (c) longitudinal profiles of the bottom topography (set of parameters: $R_p = 11000$, $\lambda_D = 0{\cdot}2$, $\beta = 30$, $\tau^* = 0{\cdot}2$, $S = 0{\cdot}02$). This figure is available in colour online at wileyonlinelibrary.com/journal/espl

Copyright © 2012 John Wiley & Sons, Ltd.

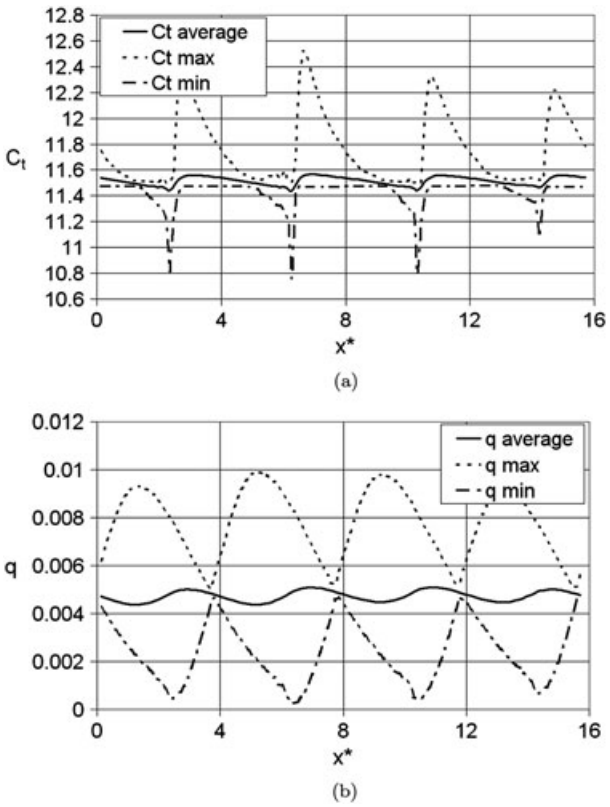

Figure 5. Example of cross-sectionally averaged total resistance C_t (a) and sediment transport q (b) for alternate bars at morphological equilibrium ($R_p = 11000$, $\lambda_D = 0{\cdot}2$, $\beta = 30$, $\tau^* = 0{\cdot}2$, $S = 0{\cdot}02$).

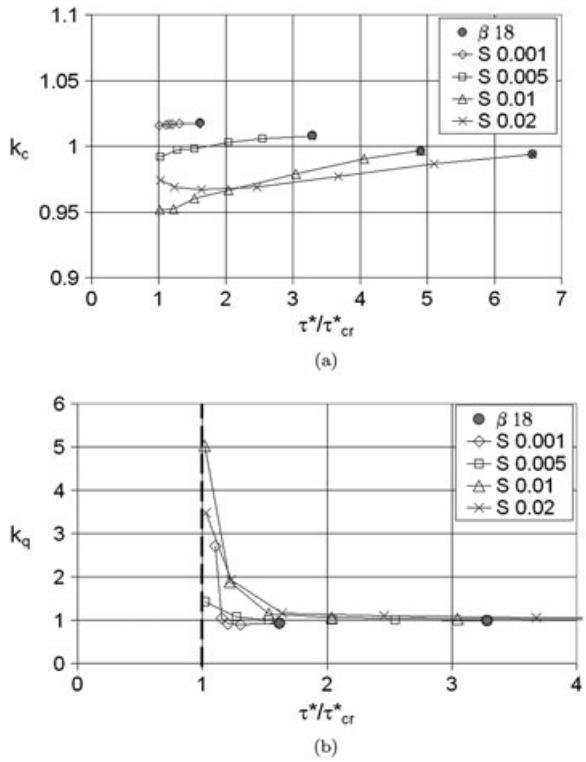

Figure 6. Correction coefficients (a) k_c and (b) k_q versus τ^*/τ^*_{cr} ranging from incipient motion to bankfull conditions, derived for four sets of parameters: $R_p = 11000$, $\lambda_D = 0{\cdot}2$, $\beta = 18$, and (τ^*, S) = (0·05, 0·001); (0·1, 0·005); (0·15, 0·01); (0·2, 0·02). The values of S are shown in the legend. Gray dots denote bankfull conditions.

hydrodynamics is numerically solved for decreasing flow depths. Such a procedure relies on the assumption that the smaller discharges do not alter significantly the bar pattern generated at bankfull flow conditions (Parker and Peterson, 1980). While this assumption may not always be accurate, it defines a useful starting point for studying the effect of below-bankfull flow.

Decreasing flow depth reduces $\bar{\tau}^*$, here we capture this effect by expressing the total resistance C_t and the bedload transport $\bar{q}$ as functions of the ratio $\bar{\tau}^*/\tau^*_{cr}$. For each topography achieved at bankfull conditions, the morphological factors k_c and k_q defined in Equations 13 and 15, respectively for C_t and $\bar{q}$, are given as a function of $\bar{\tau}^*$ in Figure 6 for the first sets of the parameters of Table I.

The parameter k_c is seen to take values ranging around one, slightly decreasing as the incipient motion condition is approached, but does not show a clear dependency on $\bar{\tau}^*$. The parameter k_q, however, ranges near unity close to the formative condition, while it increases to be several times unity as the incipient motion condition is approached. The increase of the coefficient k_q at incipient motion is modestly stronger for equilibrium topography reached at higher streamwise slope S, meaning that this latter variable may have a second order effect on the morphological factor k_q.

For the other sets of parameters, k_q only is shown, because k_c shows very similar trends in all cases. The results of the correction coefficient k_q for similar parameters but a wider channel ($\beta = 24$ and $\beta = 30$) are shown in Figure 7.

The results of the correction coefficient k_q for similar parameters but a shorter or a longer channel compared to the previous cases ($\lambda_D = 0{\cdot}1$ and $\lambda_D = 0{\cdot}4$) are shown in Figure 8.

The simulated bar topography was compared with the experimental results found from several Japanese authors as reported in the paper of Ikeda (1984), and with the experimental results of Lanzoni (2000a). The comparison, made in terms of dimensionless bar wavelength and bar height (Figure 9) as

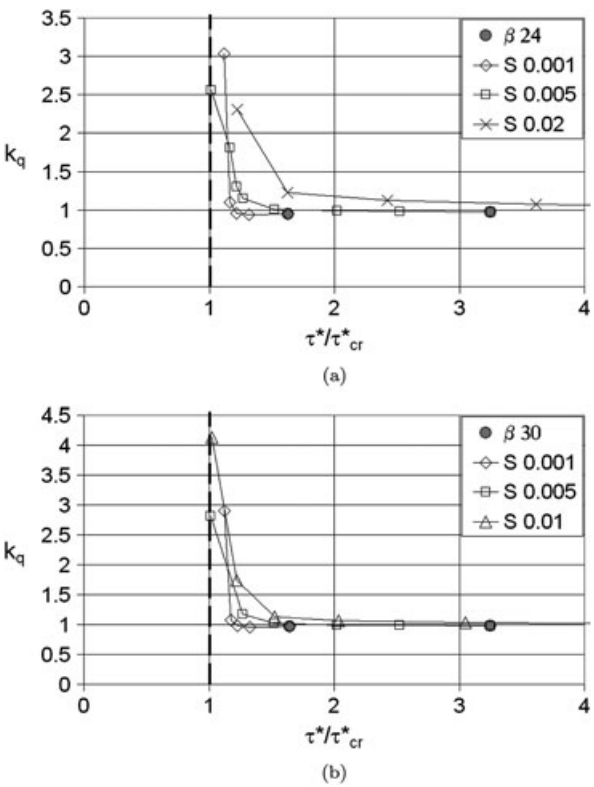

Figure 7. Correction coefficient k_q versus τ^*/τ^*_{cr} ranging from incipient motion to bankfull condition, derived for three sets of parameters: (a) $R_p = 11000$, $\lambda_D = 0.2$, $\beta = 24$, and (τ^*, S) = (0·05, 0·001); (0·1, 0·005); (0·2, 0·02); (b) $R_p = 11000$, $\lambda_D = 0{\cdot}2$, $\beta = 30$, and (τ^*, S) = (0·05, 0·001); (0·1, 0·005); (0·15, 0·01). The value of S is shown in the legend. Gray dots denote bankfull conditions.

Copyright © 2012 John Wiley & Sons, Ltd.

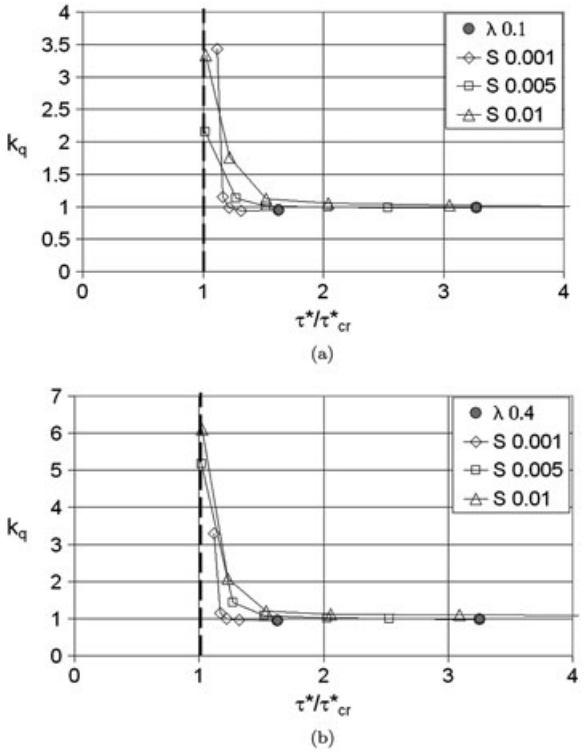

Figure 8. Correction coefficient k_q versus τ^*/τ^*_{cr} ranging from incipient motion to bankfull condition, derived for three sets of parameters: (a) $R_p = 11000$, $\lambda_D = 0{\cdot}1$, $\beta = 18$, and (τ^*, S) = (0·05, 0·001); (0·1, 0·005); (0·15, 0·01); (b) $R_p = 11000$, $\lambda_D = 0{\cdot}4$, $\beta = 18$, and (τ^*, S) = (0·05, 0·001); (0·1, 0·005); (0·15, 0·01). The value of S is shown in the legend. Gray dots denote bankfull conditions.

a function of the Shields stress, reveals that the simulated bar topography at regime morphological equilibrium has similar geometric features to the ones experimentally measured. More specifically, the data for the simulated bar topographies fall toward the center of the scatter patches of the field data.

Finally, a sensitivity analysis of the correction coefficients versus the grain roughness parameter m was conducted to verify the influence of the chosen value on the results. In the earlier calculations, the grain resistance has been estimated according to Parker (1991), using a characteristic grain roughness equal to mD_{90} with $m = 2$. This specific choice in combination with Equation 8 has been found by Wong and Parker (2006) to provide an excellent fit to the subset of the experimental data used by Meyer-Peter and Müller (1948) for which bedforms were absent. In this analysis we performed additional numerical tests, considering the first sets of the parameters of Table I, with m ranging from one to three. Results show that both correction coefficients k_c and k_q exhibit only a weak dependence on the parameter m, with trends that are almost flat (Figure 10).

These results show that alternate bars may have a strong influence on sediment transport rate. In particular, k_q attains relatively large values close to the incipient motion condition, where sediment transport rates are low. These findings suggest that the gravitational effects associated with non-negligible local longitudinal and transversal inclinations associated with alternate-bars enhance the bedload transport as the ratio $\bar{\tau}^*/\tau^*_{cr}$ decreases, but the total resistance does not vary significantly ($k_c \cong 1$). This means that mechanisms other than grain resistance acting on bedload, i.e. those associated with loss of momentum due to form drag, play a secondary role.

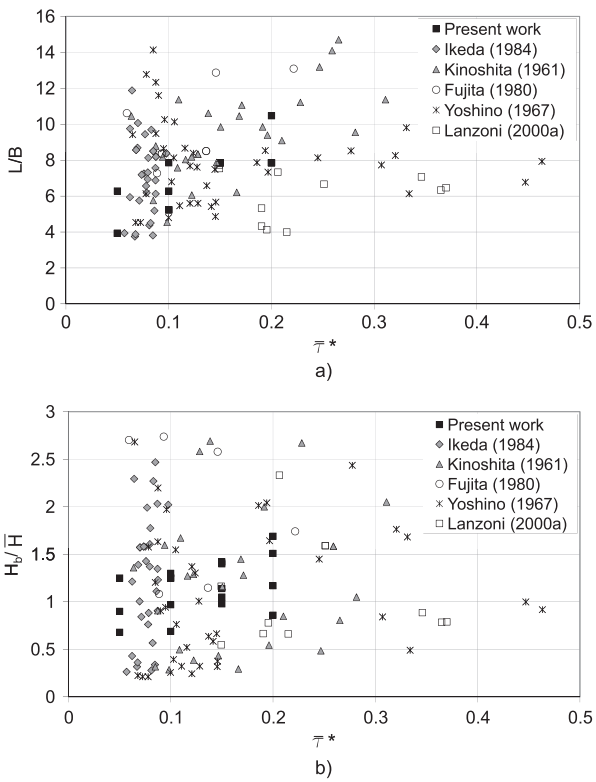

Figure 9. Comparison of alternate bar characteristic dimensions at regime morphological equilibrium with experimental data: (a) dimensionless bar wavelength L/B versus Shields stress $\bar{\tau}^*$; (b) dimensionless bar height $H_b/\bar{H}$ versus Shields stress $\bar{\tau}^*$. The legend shows the source of experimental data as from the paper by Ikeda (1984) and Lanzoni (2000a).

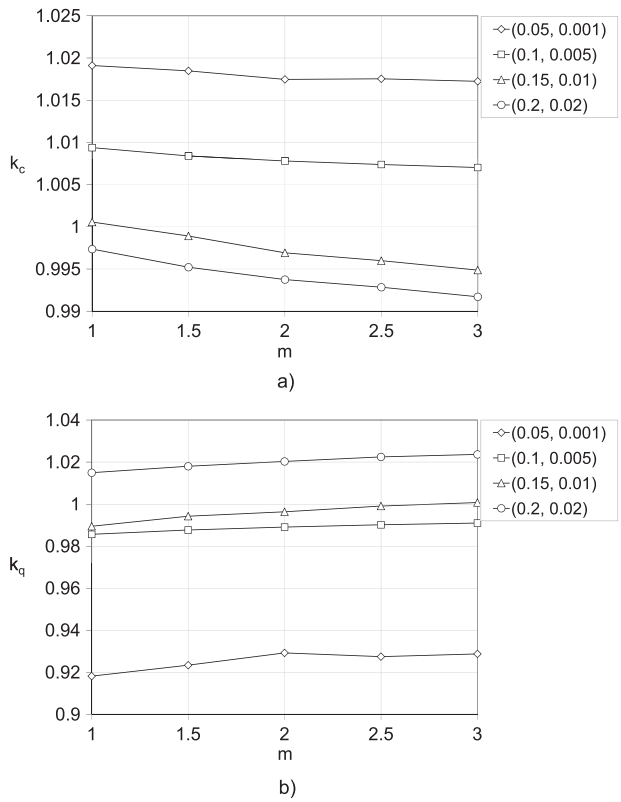

Figure 10. Correction coefficients (a) k_c and (b) k_q versus m, derived for four sets of parameters: $R_p = 11000$, $\lambda_D = 0{\cdot}2$, $\beta = 18$, and (τ^*, S) = (0·05, 0·001); (0·1, 0·005); (0·15, 0·01); (0·2, 0·02). The values of (τ^*, S) are shown in the legend.

Copyright © 2012 John Wiley & Sons, Ltd.

Discussion

Since alternate-bar patterns are characterized by both longitudinal and lateral bed oscillations, it is of interest to evaluate the morphological factors in the simple, yet non-trivial, cases of (a) a prismatic straight channel with a laterally varying cross-sectional shape (e.g. following either a linear or a sinusoidal law), and (b) a straight channel with a longitudinal bottom wave (e.g. sinusoidal) but a rectangular flat cross-section [such as in the case of schematic two-dimensional (2D) bedforms]. These cases are presented in detail with their mathematical developments in Appendices A and B. Case (a) allows an analytical solution; results for k_c and k_q are shown in Figures 11 and 12, respectively,

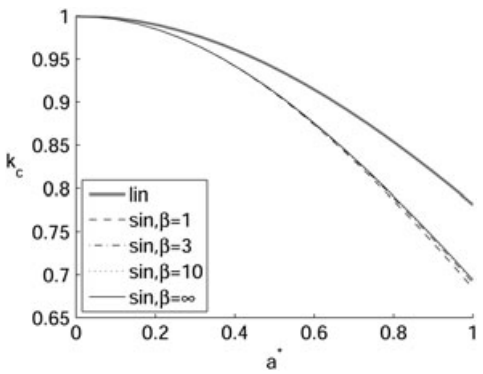

Figure 11. Correction coefficient k_c for the total resistance as a function of the dimensionless lateral amplitude a^*, in the case of uniform flow for two simplified lateral structures (see Appendix A): (lin) linear and (sin) sinusoidal lateral profile.

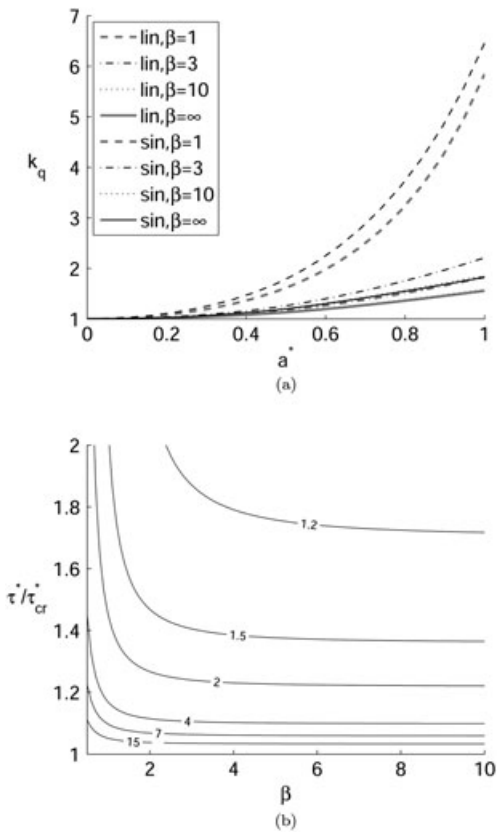

Figure 12. Correction coefficient k_q for the total bedload transport rate, for the case of uniform flow for two simplified lateral structures (see Appendix A): (a) as a function of a^* for $\bar{\tau}^*/\tau^*_{cr} = 2$ and different values of β, both for the linear and the sinusoidal lateral variation; (b) contour plot as a function of $\bar{\tau}^*/\tau^*_{cr}$ and β for the linear case with $a^* = 0{\cdot}5$.

where a^* is the amplitude of the bed variation (as defined in Appendix A), made dimensionless with water depth. It appears that a lateral variation of the flow depth in a prismatic channel produces a decrease in the flow resistance compared to the equivalent flat bed case ($k_c < 1$); this effect becomes more pronounced with increasing amplitude of lateral deformation both in the case of linear and sinusoidal variations. The sediment transport rate becomes higher ($k_q > 1$) and shows trends that are opposite to those for flow resistance. Case (b) cannot be solved analytically; the flow field is thus solved using the 3D model, with results reported in Figure 13. It appears that this bed configuration produces an increase in the flow resistance ($k_c > 1$), while the sediment transport decreases ($k_q < 1$), as shown in Appendix B.

These results can be interpreted by considering the two different effects that contribute to the total bar resistance: the lateral variation of the depth, which in all the conditions decreases the resistance, and the longitudinal variation of the bed elevation, which on the contrary produces an increase of the drag. In the case of the alternate bars, a competition between these two opposite effects comes into play. In our numerical experiments, alternate bars do not seem to appreciably affect flow resistance, thus suggesting the two opposite effects roughly balance each other. From a physical point of view, this suggests that the flow is selectively choosing routes of low resistance by moving side to side, a possibility that is not available to 2D bedforms such as dunes.

In regard to the sediment transport, the effect associated with the lateral bed oscillation dominates the longitudinal one, and the alternate-bar pattern is seen to enhance sediment transport. This is in agreement with results in Figure 12b showing that k_q attains remarkably large values with decreasing $\bar{\tau}^*/\tau^*_{cr}$; these k_q values are not compensated by the reduction of sediment transport associated with the longitudinal oscillations, because the most important element for local sediment transport is the increase of velocity occurring in the deeper regions of the bar pattern.

Previous studies (Parker and Peterson, 1980; Prestegaard, 1983), based on field observations, showed that under some conditions the overall flow resistance can be strongly affected by river bars. However, the increase in flow resistance due to river bars becomes significant only when the relative submergence is relatively low. For instance, Prestegaard (1983) estimates that bar resistance accounts for 50 to 75% of the total resistance with the relative submergence ranging between 1·69 and 7·76. Therefore, in Prestegaard's cases, flow resistance appears to be dominated by the longitudinal oscillation effect.

In our numerical experiments, the alternate bar patterns are reproduced at bankfull conditions, the relative submergence,

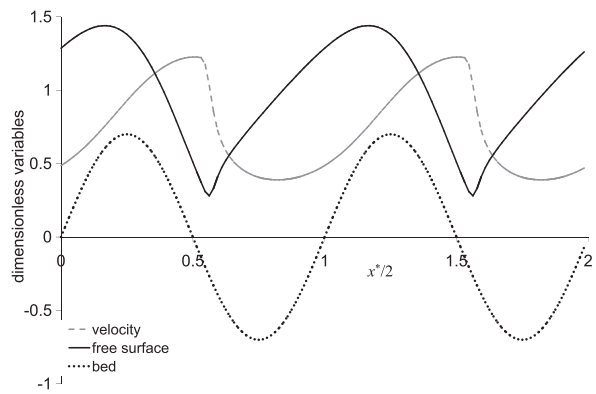

Figure 13. Numerical solution for a stationary flow over a bed with longitudinal sinusoidal oscillations: dimensionless bed elevation $\eta/\bar{H}$, free surface $H/\bar{H}$, and velocity U/U_0 (where U_0 is the reference velocity for the flat bed conditions).

Copyright © 2012 John Wiley & Sons, Ltd.

defined as ratio between the reach-averaged flow depth and the sediment size, ranges from 16·5 to 82·5 and the form drag due to bedforms is found to be negligible. Numerical experiments in the case of lower discharges and, accordingly, lower relative submergence, confirm the overall prediction of the present model, i.e. that form drag resistance remains negligible. Finally, it is important to note that we did not examine the case of bar emergence, since the numerical model does not account for wetting and drying. An effective form drag may arise when a significant portion of the bar surface is emergent at very low flow.

The earlier comment notwithstanding, our numerically-generated bars are a schematic but reasonable representation of river bars. We suggest that in nature there might be additional features not reproduced here (such as vegetation, heterogeneity of sediment size and shape and generation of smaller scale bed undulations superimposed on the bar pattern) which may alter the flow patterns from those predicted here, perhaps in ways that cause flow resistance to become dominated by the longitudinal oscillation effect, as in the case of 2D bedforms. Moreover, our numerical model does not reproduce the flow separation that can be expected at the bar front. This separation causes some energy loss, therefore increasing flow resistance. Another cause of deviation might be related to the shape of the bedforms; here, we have numerically reproduced alternate bars in a straight channel, whereas the morphology of the bars investigated in field studies is often more complex.

Conclusions

We use a 3D hydro-morphodynamic numerical model to investigate systematically how alternate bars in a straight channel affect flow resistance and sediment transport. Results are compared with those of an equivalent 1D case, which refers to flat bed conditions, but otherwise corresponding to identical reach-averaged velocity and bed slope. Our results are expressed in terms of 'morphological factors' quantifying the overall deviation of average bedload transport and flow resistance when averaged over an alternate bar wavelength, as compared to the equivalent 1D case. These 'morphological factors' can be introduced in 1D models to predict flow resistance and bedload transport over alternate bars using the classical relationships developed for flat beds.

We suggest that alternate bars can strongly enhance bedload transport at low Shields stress. However, they do not seem to alter flow resistance much. The reason for the increase in bedload transport lies in the fact that the sediment transport is nonlinearly related to local velocity, which in turn depends on the variations of the depth and on bed inclination in both the streamwise and transverse directions. The overall bedload transport rate on river bars is thus enhanced, especially in the proximity to the condition for incipient sediment motion. This condition is relatively common in gravel-bed rivers at bankfull flow (e.g. Parker *et al.*, 2007).

With regard to flow resistance, our numerical experiments show that the additional form drag due to the 3D shape of alternate bars is negligible. The reason for this behavior can be explained by decomposing the 3D geometry into transverse and longitudinal bed oscillations. The former acts to decrease the overall flow resistance, while the latter produces an increase. Bar resistance is therefore governed by the competition of two effects acting in opposite ways. In our experiments, the two effects balance each other in such a way that overall resistance is little affected by the presence of alternate bars. In natural streams, such factors as bar emergence, vegetation and channel width variation may cause additional resistance at low flow that is not captured in the present study.

Acknowledgments—The first author received financial support within the framework of the project 'Innovative methodologies for protection of river basin and coastal area (MITI)' funded by Tuscany Region (2011).

Partial support has also come from the Italian Ministry of University and of Scientific and Technological Research in the framework of the National Project 'Eco-morphodynamics of tidal environments and climate change' (PRIN 2008) cofunded by the University of Florence. The participation of the fourth author was made possible by STC program of the National Science Foundation, via the National Center for Earth-Surface Dynamics under Agreement No. EAR-0120914.

NOMENCLATURE

h= local water level with respect to the reference mean slope S
η= local bed level with respect to the reference mean slope S
H= local depth
$\bar{H}$= reach-averaged depth
H_s= equivalent flow depth for a flat bed
H_b= characteristic height of bars
x= transversal coordinate
y= longitudinal coordinate
B= channel width
S= mean streamwise slope
L= characteristic wavelength of bars
L_D= length of the periodic domain
λ= characteristic wavenumber of bars
λ_D= wavenumber of the domain
a= amplitude of lateral variation of bed elevation
k_c= morphological factor for flow resistance
k_q= morphological factor for bedload transport
U= depth-averaged velocity
$\bar{U}$= reach-averaged velocity
C_s= local skin friction coefficient
C_t= total drag coefficient
C_f= form drag coefficient
m= grain roughness parameter
τ= bed shear stress
$\bar{\tau}$= reach-averaged bed shear stress
τ^*= Shields number
$\bar{\tau}*$= reach-averaged Shields number
q= local sediment transport per unit width
$\bar{q}$ = reach-averaged sediment transport per unit width

Appendix A Prismatic Channel with Lateral Variation

We derive the analytical solution for a condition of uniform flow (steady flow in a channel with constant cross-section). From a general force balance, the total bed shear stress can be estimated as

$$\bar{\tau}\, W = \rho g A S, \tag{A1}$$

where W is the wetted perimeter of the cross-section. By means of Equation 9 we can determine the average velocity $\bar{U}$ by closing the problem with an overall resistance coefficient C_t.

However, for the simplified uniform flow case the local bed shear stress can be calculated from the 2D, depth-averaged De Saint Venant equations as

$$\tau_x(y) = \rho g S \chi(y) H(y)\ , \quad \tau_y = 0, \tag{A2}$$

with

$$\chi(y) = \left[1 + \eta_{,x}^2 + \eta_{,y}^2\right]^{-1/2}. \tag{A3}$$

Note that in the uniform case there are no longitudinal variations of the bed level with respect to the mean slope ($\eta_{,x} = 0$).

Copyright © 2012 John Wiley & Sons, Ltd.

Therefore, the total bed shear stress can be obtained by integrating the first equation in (A2),

$$\bar{\tau}\, B = \int_B \tau_x dy = \rho g S \int_B \chi H dy, \tag{A4}$$

where the effect of the banks has been neglected. Equation A4 also provides the factor $\bar{\chi}$ in Equation 9,

$$\bar{\chi} = \frac{\int_B \chi H dy}{\int_B H dy}. \tag{A5}$$

In such an ideal case, it is also possible to express the average velocity by integrating the values of the local depth-averaged velocity in the lateral direction. In fact, assuming that only the skin resistance affects the local value of the velocity, and using the closure (Equation 7) locally evaluated, the first equation in Equation A2 reduces to

$$U(y) = \sqrt{\rho g S}\left(\frac{\chi H}{C_s}\right)^{1/2}. \tag{A6}$$

Hence the cross-sectionally averaged velocity becomes

$$\bar{U} = \frac{\sqrt{\rho g S}}{B\bar{H}} \int_B C_s^{-1/2} \chi^{1/2} H^{3/2} dy, \tag{A7}$$

which can be used in Equation 6 together with Equation A4 to estimate the total resistance:

$$C_t = \int_B \chi H dy\, \bar{H}^2 B \left[\int_B C_s^{-1/2} \chi^{1/2} H^{3/2} dy\right]^{-2}. \tag{A8}$$

We introduce the dimensionless depth $H^* = H/\bar{H}$ and lateral coordinate $y^* = y/B$. We also assume for the sake of simplicity that the skin friction C_s is constant everywhere. (Accounting for variation according to a relationship such as the Manning–Strickler closure, as in the numerical model outlined earlier is straightforward, but does not change the qualitative behavior illustrated here.) The correction coefficient in Equation 13 can then be expressed in the simple form

$$k_c = \int_0^1 \chi H^* dy^* \left[\int_0^1 \chi^{1/2} H^{*3/2} dy^*\right]^{-2}. \tag{A9}$$

Assuming a linear lateral variation of the bed elevation, i.e. $H^* = 1 + a^*(1 - 2y^*)$, analytical relationships can be obtained:

$$\bar{\chi}_{lin} = \left[1 + \left(\frac{a^*}{\beta}\right)^2\right]^{-1/2}, \quad k_{c,lin} = 25a^{*2}\left[(1+a^*)^{5/2} - (1-a^*)^{5/2}\right]^{-2}. \tag{A10}$$

It is also possible to look at other simplified cases, such as a sinusoidal lateral variation $H^* = 1 + a^*\cos(\pi y^*)$. Although the solution is not analytical in this case and theoretically depends on aspect ratio β (defined with the half width), the correction $k_{c,\sin}$ can be easily calculated. The results obtained in these two simplified cases are examined in Figure 11, which shows that the total resistance diminishes as the lateral variation grows (i.e. for larger a^*), but that k_c is almost independent of β.

It is also possible to see the effect of the lateral bed variation on the sediment transport. The total sediment transport is obtained integrating Equation 14 along the width,

$$\bar{q}B = b \int_{B_a} \left(\tau^* - \tau^*_{cr}\right)^n dy, \tag{A11}$$

where B_a is the active portion of the cross-section (i.e. where $\tau^*(y) > \tau^*_{cr}$). This value can be compared with the estimate $\bar{q}(\bar{\tau}^*) = b\left(\bar{\tau}^* - \tau^*_{cr}\right)^n$ obtained using the average bed shear stress $\bar{\tau}$ or, equivalently, Shields number $\bar{\tau}^*$. Recalling Equation 15, the correction factor reads

$$k_q = \frac{1}{B}\int_{B_a} \left(\frac{\tau^* - \tau^*_{cr}}{\bar{\tau}^* - \tau^*_{cr}}\right)^n dy. \tag{A12}$$

Introducing a dimensionless critical depth H^*_{cr} (scaled with $\bar{H}$) corresponding to the critical value of the Shields number τ^*_{cr}, and assuming the exponent $n = 3/2$ of the widely used Meyer-Peter and Müller (1948) relationship, Equation (A12) can be rewritten as

$$k_q = \int_0^1 \left(\frac{H^*/H^*_{cr} - 1}{\bar{\chi}/H^*_{cr} - 1}\right)^{3/2} dy^*, \tag{A13}$$

where $\bar{\chi}/H^*_{cr} = \bar{\tau}^*/\tau^*_{cr}$ represents the degree to which the average flow deviates from critical conditions for sediment motion.

The qualitative behavior of the correction factor in this simplified case is shown in Figure 12, from which it is clear that the total transport can become significantly larger than the estimate made with parameters based on average hydrodynamics.

Appendix B Longitudinally Varying Channel with Rectangular Cross-section

Having explored the effect of lateral variations of the bed in Appendix A, we now discuss the alternative case for which only longitudinal variations exist. This case can be tackled by means of 1D numerical models, but in this section we show the results of an application of the complete 3D model to this simplified case. Assuming steady conditions and neglecting the effect of the banks as a first approximation, the simplified problem is described by the depth-averaged differential equation

$$\left(1 - F_r^2\right)\frac{dH}{dx} - S + C_s F_r^2 = 0, \tag{B1}$$

where the Froude number F_r is a function of the depth H (constant along the cross-section).

The problem can be studied with an imposed longitudinally varying bed. Looking for a significant yet simple case, we assume a sinusoidal law for the variation of the bed elevation with respect to the bed profile corresponding to the mean slope;

$$\eta = a\cos(\lambda x^*), \tag{B2}$$

where the wavenumber λ is defined in analogy with Equation 19, and hence x^* is made dimensionless with the half width. This problem does not admit an analytical solution.

Figure 13 shows the numerical result for a test case, where $a/\bar{H} = 0{\cdot}7$ and $\lambda = 0{\cdot}4$. It is evident that the flow field is strongly affected by the strong variation in bed elevation. (We have purposely chosen a very large amplitude of bed oscillation in order

Copyright © 2012 John Wiley & Sons, Ltd.

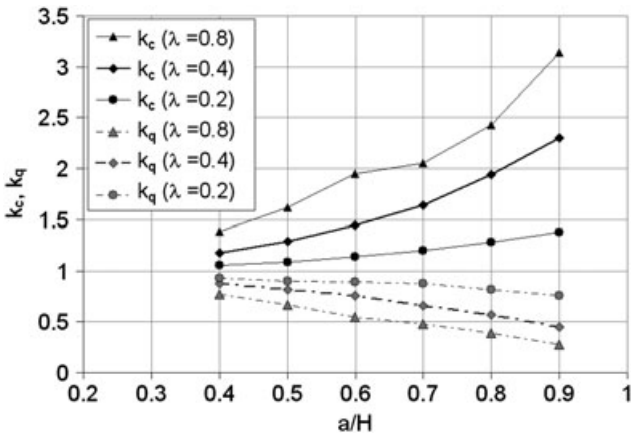

Figure 14. Correction coefficients k_c and k_q versus the dimensionless amplitude of the bed oscillation $a/\bar{H}$, for different values of the wavenumber λ.

to make the behavior more evident.) As a result, the total resistance strongly increases ($k_c = 1{\cdot}64$) and the total sediment transport rate decreases ($k_q = 0{\cdot}66$). Similarly to the case of lateral variations, a series of numerical tests was conducted to evaluate the correction coefficients k_c and k_q as functions of the amplitude of the bed oscillation, and of the wavenumber λ. Results, reported in Figure 14, show that k_c is always higher than one, and that it increases with the amplitude of oscillation $a/\bar{H}$. The total sediment transport, however, is always decreasing. In addition, it was found that bed deformations with higher wavenumber correspond to greater changes in the correction coefficients.

The comparison between the simplified tests in the Appendices shows that, while lateral variations of the bed elevation typically decrease the total drag coefficient, longitudinal oscillations of the bed tend to increase it. In the presence of alternate bars, the two phenomena have opposite effects and tend to counter each other, because the alternate bar topography is characterized by oscillations of the bed elevation both in the longitudinal and transversal directions.

References

Bathurst JC. 1981. Discussion of 'bar resistance of gravel-bed streams'. *Journal of the Hydraulics Division, ASCE* **107**: 1276–1278.

Blanckaert K. 2009. Saturation of curvature-induced secondary flow, energy losses, and turbulence in sharp openchannel bends: laboratory experiments, analysis, and modelling. *Journal of Geophysical Research* **114**: F03015. DOI: 10.1029/2008JF001137

Blanckaert K, de Vriend HJ. 2003. Nonlinear modeling of mean flow redistribution in curved open channels. *Water Resources Research* **39**(12): 1375. DOI: 10.1029/2003WR002068

Colombini M, Seminara G, Tubino M. 1987. Finite-amplitude alternate bars. *Journal of Fluid Mechanics* **181**: 213–232.

Dinehart RL. 1989. Dune migration in a steep, coarse-bedded stream. *Water Resources Research* **25**(5): 911–923.

Einstein HA. 1950. The Bed-load Function for Sediment Transportation in Open Channel Flows, Technical Bulletin 1026. US Department of the Army, Soil Conservation Service: Washington, DC.

Einstein HA, Barbarossa NL. 1952. River channel roughness. *Transactions of the American Society of Civil Engineers* **117**: 1121–1146.

Engelund F, Hansen E. 1967. A Monograph on Sediment Transport in Alluvial Streams. Technisk Vorlag: Copenhagen.

Francalanci S, Solari L. 2008. Bed-load transport equation on arbitrarily sloping beds. *Journal of Hydraulic Engineering* **134**(1) 110–115.

Francalanci S, Solari L, Toffolon M. 2009. Local high-slope effects on sediment transport and fluvial bed form dynamics. *Water Resources Research* **45**: W05426. DOI: 10.1029/2008WR007290

Ikeda S. 1984. Prediction of alternate bar wavelength and height. *Journal of Hydraulic Engineering* **110**(4): 371–386.

Kaufmann PR, Faustini JM, David P, Larsen DP, Shirazi MA. 2008. A roughness-corrected index of relative bed stability for regional stream surveys. *Geomorphology* **99**: 150–170.

Lanzoni S. 2000a. Experiments on bar formation in a straight flume. Part I: Uniform sediment. *Water Resources Research* **36**(11): 3337–3349.

Lanzoni S. 2000b. Experiments on bar formation in a straight flume. Part II: Graded sediment. *Water Resources Research* **36**(11): 3351–3363.

Madej MA, Sutherland DG, Lisle ET, Pryor B. 2009. Channel responses to varying sediment input: a flume experiment modeled after Redwood Creek, California. *Geomorphology* **103**(4): 507–519. DOI: 10.1016/j.geomorph.2008.07.017

Meyer-Peter E, Müller R. 1948. Formulas for bed-load transport. Proceedings, 2nd Meeting, IAHR, Stockholm; 39–64.

Millar RG. 1999. Grain and form resistance in gravel-bed rivers. *Journal of Hydraulic Research* **37**(3): 303–312.

Paola C, Seal R. 1995. Grain size patchiness as a cause of selective deposition and downstream fining. *Water Resources Research* **31**(5): 1395–1407.

Parker G. 1991. Selective sorting and abrasion of river gravel. II: Applications. *Journal of Hydraulic Engineering* **117**(2): 150–171.

Parker G. 2004. 1D Sediment Transport Morphodynamics with applications To Rivers and Turbidity Currents. Copyrighted e-book downloadable from: http://vtchl.uiuc.edu/people/parkerg/

Parker G. 2008. Transport of gravel and sediment mixtures, Chapter 3. In Sedimentation Engineering: Processes, Measurements, Modeling and Practice, Garcia MH (ed.), ASCE Manual of Practice 110. American Society of Civil Engineers: Reston, VA; 165–252.

Parker G, Peterson AW. 1980. Bar resistance of gravel-bed streams. *Journal of the Hydraulic Division* **106**(10): 1559–1575.

Parker G, Wilcock PR, Paola C, Dietrich WE, Pitlick J. 2007. Physical basis for quasi-universal relations describing bankfull hydraulic geometry of single-thread gravel bed rivers. *Journal of Geophysical Research* **112**: F04005. DOI: 10.1029/2006JF000549

Prestegaard KL. 1983. Bar resistance in gravel bed streams at bankfull stage. *Water Resources Research* **19**(2): 472–476.

Toffolon M, Vignoli G. 2007. Suspended sediment concentration profiles in nonuniform flows: is the classical perturbative approach suitable for depth-averaged closures? *Water Resources Research* **43**: W04432. DOI: 10.1029/2006WR005183

Vignoli G. 2005. Modelling the Morphodynamics of Tidal Channels. University of Trento: Trento; 129 pp. http://www.unitn.it/files/monographs_7.pdf

Vignoli G, Tubino M. 2002. A numerical model for sand bar stability. Proceedings of the International Conference on Fluvial Hydraulics, River Flow 2002, Louvain-La-Neuve, Belgium, 4–6 September, vol. **2**, Bousmar D, Zech Y (eds). Swets and Zeitlinger: Lisse; 833–841.

Wong M, Parker G. 2006. Reanalysis and correction of bed-load relation of Meyer-Peter and Müller using their own database. *Journal of Hydraulic Engineering* **132**(11): 1159–1168. DOI: 10.1061/(ASCE)0733-9429(2006)132:11(1159)

Copyright © 2012 John Wiley & Sons, Ltd.